The Metamer Boundary Descriptor Method for Color Correction

Philipp Urban
Ratio Entwicklungen GmbH, Hamburg, GERMANY

Rolf-Rainer Grigat▲
Hamburg University of Technology, Vision Systems, Hamburg, GERMANY

Color correction describes the transformation process between device response values, e.g., RGB, and CIE XYZ or CIE L*a*b* values, respectively. In every metamer color reproduction system this is the first color transformation after image acquisition. In general, this mapping is not unique because the spectral sensitivities of the majority of devices do not satisfy the Luther condition and the acquisition and viewing light sources typically have different power spectra. Hence, there exists a set of colors with different reflectance spectra which result in the same device response (device metamerism), but have different CIE XYZ tristimulus values for an observer under the viewing light source. In this publication we present a new method to determine this metamer subspace (which depends on the device response) in the viewing CIE L*a*b* space by calculating a Metamer Boundary Descriptor (MBD) matrix. This MBD matrix approximately describes the metamer subspace by storing its boundary points in every entry. By calculating the center of gravity of this MBD we obtain a good color choice in the sense of a small mean error. To calculate the entries of the MBD we use *a priori* knowledge about the physics of natural reflectance spectra and a linear programming technique. This method improves the performance of target- and regression-based methods especially for saturated colors. We present the results of simulation experiments including a comparison with existing methods.

Journal of Imaging Science and Technology 49: 418–430 (2005)

Introduction

In every metamer color reproduction system color correction, i.e., the mapping from device response values, e.g., RGB, to CIE XYZ or CIE L*a*b* colors, respectively, is the first color transformation after image acquisition.

There are two different classes of methods for color correction in linear acquisition systems: target based methods and model based methods. Target based methods use a set of sample CIE XYZ/CIE L*a*b* colors with corresponding sensor responses to determine an approximation of the color correction transformation. The best known method is the linear mapping between the sensor response values and CIE XYZ colors. Assuming that the CIE XYZ colors depend linearly on sensor response values this transformation must be optimal. If we consider acquisition systems with $q \geq 3$ channels and sensor response space C the linear method determines a transformation $3 \times q$ matrix A, using linear regression of the target colors. The color correction transformation can be written as follows

$$A \cdot c = (X, Y, Z)^T, \tag{1}$$

where $c \in C$ is an arbitrary sensor response.

As a result of different acquisition and viewing light sources and non-compliance of the Luther condition, i.e., the linear dependency of the CIE color matching functions on system sensitivities,[1,2] by the spectral sensitivities of the image acquisition system the transformation is generally not linear and the method results in high ΔE errors.

In order to consider these non-linear effects in the color correction transformation the use of polynomial mapping of order $p > 1$ would appear to represent an improvement:[3]

$$\begin{bmatrix} P_X(c) \\ P_Y(c) \\ P_Z(c) \end{bmatrix} = (X, Y, Z)^T, \tag{2}$$

where

$$P_x(c = (c_1, \ldots, c_q)^T) = \sum_{i_1 + \cdots + i_q \leq p} a^x_{(i_1, \ldots, i_q)} \prod_{j=1}^{q} c_j^{i_j}, \tag{3}$$

for $x = X, Y, Z$. The coefficients $a^x_{(i_1, \ldots, i_q)}$ can be calculated using multi-order polynomial regression (MPR) of the target colors.

Original manuscript received January 12, 2004

▲ IS&T Member

†Corresponding Author: P. Urban, urban@tu-harburg.de

Supplemental Material— Appendix A and Appendix B can be found on the IS&T website (www.imaging.org) for a period of no less than two years from the date of publication.

In the methods described above the regression was calculated in the intensity-linear CIE XYZ color space. This minimizes the root mean square (RMS) difference between the mapped CIE XYZ colors and the corresponding CIE XYZ target colors. Unfortunately, Euclidean distances in CIE XYZ are very poorly correlated to visual color differences.[4] A common nearly perceptual uniform color space is the CIE L*a*b* space in which the euclidean distance is the ΔE^*_{ab} color difference formula. Therefore, if the regression can be performed directly in the CIE L*a*b* color space, this should lead to an improvement with respect to small ΔE^*_{ab} values.

Hardeberg[3] initially transformed R, G, B sensor responses with a nonlinear function $g(x) = x^{1/3}$ to achieve a nearly linear relationship between the $g(R)$, $g(G)$, $g(B)$ values and the CIE L*a*b* colors. This leads to a better performance of the subsequent multi-order polynomial regression and smaller ΔE errors. The reason for choosing $g(x) = x^{1/3}$ is the transformation formula between CIE XYZ and CIE L*a*b*. We call the method "multi-order polynomial regression into CIE L*a*b* based on Hardeberg" (MPRLabH). A generalization to q channel systems can be performed by initially transforming each channel response by $g(x)$

$$\begin{bmatrix} P_{L^*}(g(c_1),...,g(c_q)) \\ P_{a^*}(g(c_1),...,g(c_q)) \\ P_{b^*}(g(c_1),...,g(c_q)) \end{bmatrix} = (L^*, a^*, b^*)^T, \tag{4}$$

where P_x, $x = L^*, a^*, b^*,$ are similarly defined as in Eq. (3).

König[5] transformed the sensor response values as in Eq. (1), but subsequently performed a multi-order polynomial regression to the real target CIE L*a*b* colors

$$A \cdot c = (X, Y, Z)^T \rightarrow (\tilde{L}^*, \tilde{a}^*, \tilde{b}^*)^T \rightarrow \begin{bmatrix} P_{L^*}(\tilde{L}^*, \tilde{a}^*, \tilde{b}^*) \\ P_{a^*}(\tilde{L}^*, \tilde{a}^*, \tilde{b}^*) \\ P_{b^*}(\tilde{L}^*, \tilde{a}^*, \tilde{b}^*) \end{bmatrix} = (L^*, a^*, b^*)^T, \tag{5}$$

where P_x, $x = L^*, a^*, b^*,$ are similarly defined as in Eq. (3). We call this method "multi-order polynomial regression into CIE L*a*b* based on König" (MPRLabK).

If we consider noisy systems the regression-based methods result in high error rates. König[5] proposed a new matrix based method as in Eq. (1) by calculating the coefficients using linear programming. The aim of the calculation is to achieve matrix entries which have nearly the same size but still cause small errors. The resulting matrix does not amplify the noise as much as regression-based matrices. We call the method "robust matrix" method (RM).

Other different target based methods have been developed and proposed for color correction using neural networks,[6] LUT-interpolation and extrapolation[7] or constraint least square-regression to preserve the white point,[8] to name a few.

The other class of color correction methods involves model based methods. These methods use the mathematical model of the image acquisition system (which will be discussed below) to reconstruct the CIE L*a*b* colors from the sensor response values. As mentioned earlier the acquisition and viewing light can differ and spectral sensitivities of the image acquisition system might not satisfy the Luther condition. Therefore, the reconstruction is generally not unambiguous. There are various colors with different reflectance spectra which result in the same device response (device metamerism), but have different CIE XYZ tristimulus values for an observer under the viewing light source. These values form the "metamer subspace" with respect to the device response.

One method is to reconstruct a reflection spectrum from the sensor response of the acquisition system and to calculate the appropriate CIE XYZ color. Several methods have been proposed to perform this reconstruction such as Pseudoinverse, smoothing Inverse,Wienerinverse or Principle Component Analysis (PCA) (see, e.g., Refs. 3, 5, and 9). For acquisition systems using only a few channels, e.g., RGB, the set of possible spectra leading to the given sensor response is very extensive because there are many degrees of freedom to reconstruct the reflection spectrum (metameric black space,[10] see below). This can result in large ΔE errors.

One of these reconstruction methods is the procedure involving "projection onto convex sets" (POCS) which can be used in many fields of color science.[11,12] This method finds a feasible spectrum in the intersection of some convex sets which define constraints such as positivity, boundedness, smoothness and "leading to the sensor response". The resulting spectrum defines an arbitrary tristimulus value in the metamer subspace which depends on the starting point of the POCS iteration. As mentioned above the metamer subspace can be very large for acquisition systems with only a few channels, so additional constraints can be used if, e.g., the model of the printer creating the acquired color is known *a priori*.[13,14]

Finlayson and Morovic[15] attempted to characterize the metamer subspace of possible color spectra which result in the given sensor response in the viewing CIE XYZ space. They used a linear programming technique to find the smallest cube in which the metamer subspace is located and chose the center of this cube for color correction (Linear Programming Center of Cube – LPCC). They also proposed a different technique to determine the desired color by sampling this cube (as a region of interest) to find feasible points and take the centroid of the feasible set. The center of gravity of the metamer subspace in the CIE XYZ color space generally differs from the center of gravity of the set in the CIE L*a*b* color space, where the common ΔE metrics are defined. If the aim of a color correction transformation is to minimize the ΔE color difference between the real color and the calculated color, an inspection of the metamer subspace in the CIE L*a*b* color space seems to be more effective. Furthermore, the description of the metamer subspace using an enveloping cube is only a very rough characterization.

The list of model-based methods is not exhaustive. It should be mentioned that there are some methods which use the image acquisition model to calculate a matrix based color correction as in Eq. (1).[16–18]

In this publication we propose a method that characterizes the metamer subspace in the nearly perceptual uniform CIE L*a*b* color space by calculating a metamer boundary descriptor matrix. The center of gravity of the matrix entries is an approximation of the color with the smallest ΔE distance to all other colors in the metamer subspace. This color is the optimal color choice for color correction in the sense of small mean error.

The Metamer Subspace

In this section we define the metamer subspace of a sensor response for different acquisition and viewing

illuminants and also show that a color correction transformation is generally not unambiguous.

In a linear acquisition system the relationship between the acquisition illuminant L_a, the sensitivities $s_1,\ldots,s_q$, the reflection spectrum r, and the sensor response $c = (c_1,\ldots,c_q)^T \in C$, is as follows

$$c_i = \int_\Lambda s_i(\lambda)L_a(\lambda)r(\lambda)d\lambda + \varepsilon, \quad i = 1,\ldots,q, \tag{6}$$

where Λ = [400 nm, 700 nm] is the visible wavelength interval and ε is the additive noise.

The corresponding discrete formulation achieved by sampling the spectra in N equal wavelength intervals is given by

$$c = \Omega_a r + \varepsilon \tag{7}$$

where $r = (r(\lambda_1),\ldots,r(\lambda_N))^T$ and the acquisition lighting matrix

$$\Omega_a = \begin{bmatrix} s_1(\lambda_1)L_a(\lambda_1) & \cdots & s_1(\lambda_N)L_a(\lambda_N) \\ \vdots & & \vdots \\ s_q(\lambda_1)L_a(\lambda_1) & \cdots & s_q(\lambda_N)L_a(\lambda_N) \end{bmatrix}$$

In this article the sensor response $c \in C$, the acquisition light L_a and the system sensitivities $s_1,\ldots,s_q$ are well-known.

In practice the system sensitivities have to be determined by measurement or by using a set of training colors and a reconstruction method, e.g., Pseudoinverse, Wiener-inverse,[19] Principle Eigenvector,[3] Projection onto Convex Sets,[12,20] Linear Programming,[5] and Quadratic Programming.[21]

Given the same reflection spectrum r an observer's tristimulus value $v_r \in$ CIE XYZ for the viewing illuminant L_v can be modeled in an analogous manner as the sensor response. Here we present only the discrete form

$$v_r = \Omega_v r \tag{8}$$

where Ω_v is the observer lighting matrix depending on the CIE color matching functions $\bar{x}, \bar{y}, \bar{z}$.

$$\Omega_v = \begin{bmatrix} \bar{x}(\lambda_1)L_v(\lambda_1) & \cdots & \bar{x}(\lambda_N)L_v(\lambda_N) \\ \bar{y}(\lambda_1)L_v(\lambda_1) & \cdots & \bar{y}(\lambda_N)L_v(\lambda_N) \\ \bar{z}(\lambda_1)L_v(\lambda_1) & \cdots & \bar{z}(\lambda_N)L_v(\lambda_N) \end{bmatrix}.$$

Solving Eq. (7) with respect to the reflection spectrum r results in

$$r = \Omega_a^\Theta(c - \varepsilon) + \text{Kernel}(\Omega_a) \tag{9}$$

where Ω_a^Θ is the pseudo-inverse matrix of Ω_a and $\text{Kernel}(\Omega_a) := \{w \mid \Omega_a w = 0\}$. By analogy to human colorimetry the fundamental metamer is represented by $\Omega_a^\Theta(c - \varepsilon)$ and $\text{Kernel}(\Omega_a)$ is the space of metameric blacks of the device.[10,22,23]. If we construct a matrix $W := (w_1,\ldots,w_K)$ using a basis $w_1,\ldots, w_K$ of $\text{Kernel}(\Omega_a)$ we can rewrite Eq. (9) as follows

$$r = \Omega_a^\Theta(c - \varepsilon) + Wu,\ u \in \mathbb{R}^K \tag{10}$$

This algebraic solution must be restricted by physical conditions such as the positivity, boundedness and smoothness of r (see, e.g., Refs. 10, 24, and 25). So not all $u \in \mathbb{R}^K$ are physically useful. $U \subset \mathbb{R}^K$ denotes the subset that fulfils these constraints in Eq. (10). If we insert Eq. (10) in Eq. (8), we obtain the metamer set M^c_{XYZ} of possible tristimuli in the CIE XYZ color space

$$M^c_{XYZ} = \{\Omega_v\Omega_a^\Theta(c - \varepsilon) + \Omega_v W u \mid u \in U\}. \tag{11}$$

The ΔE error metrics (color difference formulas) are defined in the CIE L*a*b* color space, so we map the elements of M^c_{XYZ} from the intensity-linear CIE XYZ color space into the nearly perceptual uniform CIE L*a*b* space. We denote this transformation by $\mathcal{L}$: CIE XYZ $\mapsto$ CIE L*a*b* and define our metamer subspace by

$$M^c_{Lab} = \mathcal{L}(M^c_{XYZ}). \tag{12}$$

To calculate the metamer subspace M^c_{XYZ} different methods have been proposed and described.[10] Apart from Monte Carlo calculations (using random metameric reflection spectra or reflection spectra derived by the metameric black method[10]), a linear programming method has also been developed.[26] These methods do not consider the smoothness characteristic of natural reflection spectra, which generally leads to larger metamer subspaces. Furthermore, they characterize the metamer subspace in the CIE XYZ color space.

The Optimal Color Correction Transformation

In this section we define the optimal color correction transformation in the sense of the minimal mean error.

We show above that a color correction transformation is in general not unambiguous. For a given sensor response c each color of the metamer subspace M^c_{Lab} is a possible choice for color correction, but only one color in this metamer subspace is actually created by the acquired surface with unknown reflection spectrum. If we choose an arbitrary color $x \in M^c_{Lab}$ there is at least one reflection spectrum r which results in the sensor response c and a color $y \in M^c_{Lab}$ where

$$\Delta E(x, y) = \max_{z \in M^c_{Lab}} \Delta E(x, z). \tag{13}$$

One aim of a color correction transformation could be the selection of a color $x \in M^c_{Lab}$ which minimizes this maximal error. If we focus on the minimization of mean error we obtain the following definition for an optimal color correction transformation:

Definition 1 (Optimal Color Correction Transformation)

We assume a linear sensor response $c \in C$ for an acquisition illuminant a (see Eq. (7)) and the appropriate metamer subspace M^c_{Lab} for the viewing illuminant v (see Eq. (12)) with the probability density function $\delta : M^c_{Lab} \mapsto [0, 1]$ of metamers in M^c_{Lab} fulfilling

$$\int_{M^c_{Lab}} \delta(x)dx = 1. \tag{14}$$

A color correction transformation $C : C \mapsto$ CIE L*a*b* is optimal for the sensor response c with respect to a color difference metric ΔE : CIE L*a*b* $\times$ CIE L*a*b* $\mapsto \mathbb{R}^+_0$, if the following equation applies:

$$C(c) = \arg\left(\min_{x \in M^c_{Lab}} \int_{M^c_{Lab}} \delta(x)\delta(y)\Delta E(x,y)dy \right). \quad (15)$$

A color correction transformation is optimal with respect to a color difference metric ΔE if Eq. (15) applies for all $c \in C$.

It is difficult to determine the minimum in Eq. (15), so we are satisfied with an approximation of this color with respect to the ΔE^*_{ab} metric by selecting the center of gravity of the metamer subspace M^c_{Lab}. The calculation of the probability density function δ of metamers inside the metamer subspace is also difficult. A Monte Carlo calculation of the boundary of M^c_{XYZ} made by Ohta[10] considers a normal trivariate distribution of metamers inside M^c_{XYZ}. This assumption is based on previous research which involved counting metamers inside the object-color solid.[10,24] Transformation of the normal distributed points in M^c_{XYZ} into CIE L*a*b* changes the skewness and kurtosis of their distribution. Hence we do not know the parameters of the normal distribution of the points in M^c_{XYZ} *a priori* and to avoid the complex calculation of transforming its density function for M^c_{Lab} we do not consider the distribution of the points. So the optimal color correction choice as defined by Eq. (15) differs from our solution due to our choice of the center of gravity of the metamer subspace with equally distributed points. Nevertheless, the shape of the metamer subspace M^c_{Lab} is important for both calculations – the optimal calculation in definition 1 and the approximate calculation using the simplified center of gravity. In the next Section we will present a method which characterizes this subspace by virtue of a metamer boundary descriptor.

The Metamer Boundary Descriptor

The Metamer Boundary Descriptor (MBD) is a $n \times m$ matrix which stores a boundary point of the metamer subspace M^c_{Lab} in every entry. Each row contains m contour points of the set with a fixed L^* value. The boundary points are calculated in the CIE XYZ space using Linear Programming (LP). A short overview of LP is given in Appendix A, available as Supplemental Material.

The main idea of this article is to formulate the following LP problem, which samples the boundary of the metamer subspace along an arbitrary straight line $g + \lambda v$ (see explanations below and Fig. 1)

$$-\lambda = \min \quad (16)$$

with the linear constraints

$$r \geq 0 \quad (17)$$

$$r \leq 1 \quad (18)$$

$$Hr \leq \rho \quad (19)$$

$$-Hr \leq \rho \quad (20)$$

$$\Omega_a r = c + \varepsilon \quad (21)$$

$$\Omega_v r = v_r \quad (22)$$

$$g + \lambda v = v_r \quad (23)$$

$$\lambda \geq 0 \quad (24)$$

Constraint (17) ensures the positivity of reflectance spectra and constraint (18) guarantees the boundedness

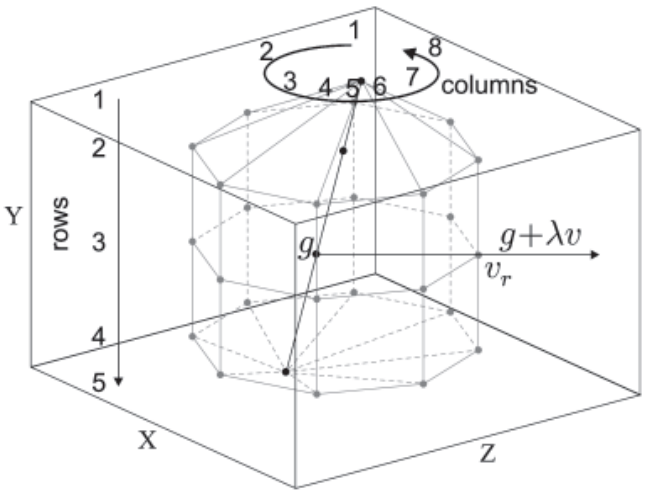

Figure 1. Sampling of the metamer subspace M^c_{XYZ} along the line $g + \lambda v$, $\lambda \geq 0$. The corresponding MBD matrix has 8 columns and 5 rows.

of non-fluorescent surfaces (see e.g., Refs. 10, 15, and 26). In addition, we employ the smoothness constraint (used in Ref. 20, to assure smooth scanner sensitivities) in Eqs. (19) and (20) with a smoothing parameter $\rho > 0$ and a convolution matrix H to apply the Laplace operator to r:

$$H = \begin{bmatrix} 1 & -2 & 1 & & \\ & \ddots & \ddots & \ddots & 0 \\ 0 & & 1 & -2 & 1 \end{bmatrix} \quad (25)$$

Constraint (21) ensures that we only take reflectance spectra r into account, which lead to the given sensor response $c + \varepsilon$. Constraint (22) introduces the observer's lighting matrix with the auxiliary variable v_r. Constraints (17) through (22) define the metamer subspace M^c_{XYZ}. In other words, for each reflection spectrum which fulfils all these constraints the resulting auxiliary variable v_r lies in M^c_{XYZ} and for each point in M^c_{XYZ} there is a reflection spectrum which fulfils the constraints. The next constraint (23) restricts the auxiliary variable $v_r \in M^c_{XYZ}$ so that it lies on the sampling line defined by g and v. We are looking for the point $v_r \in M^c_{XYZ}$ on the line with a maximum positive λ in order to find a boundary point of the convex set M^c_{XYZ} (see Fig. 1). The notation λ = max could be expected as the objective function, but the mathematical convention (see Appendix A) is the minimization of the objective function which leads to the above objective function, Eq. (16).

By solving this LP we obtain a tristimulus value v_r, which is the intersection of the line and the boundary of M^c_{XYZ}, and the appropriate reflection spectrum r. Since all constraints form a convex set, there is only one intersection point v_r. This intersection point has to be transformed into CIE L*a*b* coordinates and stored in the MBD matrix.

After calculating the MBD matrix the color correction can be realized by choosing the center of gravity of the points in the matrix (see below and Appendix B, available as Supplemental Material).

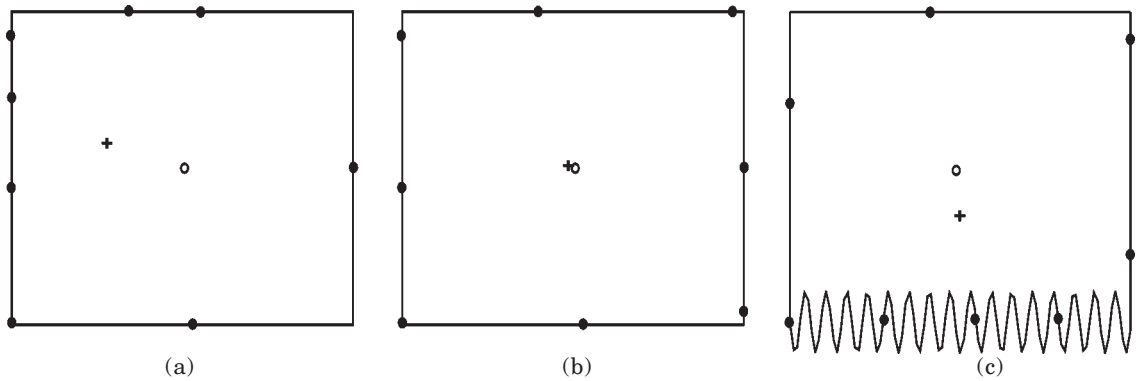

Figure 2. Effects on the accuracy of the calculated center of gravity of some sets using points on their boundaries. Cross = center of gravity of the points. Circle = Center of gravity of the set. a) Points are not uniformly distributed on the boundary of the set; b) points are uniformly distributed on the boundary of the set; and c) points are uniformly distributed on the boundary of the set, but the shape of the boundary is not uniformly structured.

The accuracy of the calculated center of gravity of the metamer subspace using points on its boundary is generally enhanced by uniformly distributed points (see Fig. 2(a) and 2(b)). The influence of a non-uniformly structured boundary shape as shown in Fig. 2(c) is not very strong because the transformation of the convex set M^c_{XYZ} (which has a uniformly structured boundary shape) by the smooth function $\mathcal{L}$ does not add any appreciable structure to its boundary. Therefore, for each boundary point the parameters g and v, which define the sampling line, have to be chosen so that the MBD entries are uniformly distributed on the boundary of M^c_{Lab}. A construction scheme of the half line parameters g and v, which result in nearly uniformly distributed points in the MBD matrix, is described next.

Flexible sampling of the metamer subspace along an arbitrary line is one of the differences from the LP method[10,26] and permits a better description of the metamer subspace in the CIE L*a*b* color space.

To solve the LP problems we used the optimization toolbox of Matlab,[27] which employs a variation of the predictor-corrector algorithm from Mehrotra.[28]

Half Line Parameter

Here we describe a construction scheme for the half line parameters g and v used in constraint (23) which result in sampling points with an almost uniform distribution on the boundary of M^c_{Lab}.

As mentioned in the previous section the sampling points have to be chosen so that they are uniformly distributed on the boundary of M^c_{Lab}. As the metamer subspace is sampled in the CIE XYZ color space certain calculations are necessary.

Anchor Point g

All half lines used to determine a MBD row have the same anchor point g (Fig. 1). We therefore only have to calculate n anchor points g_i, $i = 1,\ldots,n$ for a $n \times m$ MBD matrix. We select the anchor points in such a way that they uniformly cover the luminance spread of M^c_{Lab}. To determine this luminance spread we have to solve the following two LP problems

$$-v_r^Y r = \min \tag{26}$$

$$v_r^Y r = \min, \text{ resp.} \tag{27}$$

with the linear constraints

$$r \geq 0 \tag{28}$$

$$r \leq 1 \tag{29}$$

$$Hr \leq \rho \tag{30}$$

$$-Hr \leq \rho \tag{31}$$

$$\Omega_a r = c + \varepsilon \tag{32}$$

$$\Omega_v r = v_r \tag{33}$$

The LP problem with the objective function (26) results in a color $v_{r,\max} \in M^c_{XYZ}$ with a maximal Y value. The LP problem with the objective function (27) leads to $v_{r,\min} \in M^c_{XYZ}$ with a minimal Y value. We transform both colors into the CIE L*a*b* space to get the luminance spread of M^c_{Lab}.

$$[L^*_{\min}, L^*_{\max}] := [\mathcal{L}_{L^*}(v_{r,\min}), \mathcal{L}_{L^*}(v_{r,\max})] \tag{34}$$

and sample this interval at n equidistant positions

$$L^*_i := L^*_{\min} + \frac{i-1}{n-1}\left(L^*_{\max} - L^*_{\min}\right), \; i = 1,\ldots,n. \tag{35}$$

We can now define the desired anchor points in the CIE XYZ space as follows

$$g_i := v_{r,\min} + \frac{Y_i - Y_1}{Y_n - Y_1}\left(v_{r,\max} - v_{r,\min}\right), \tag{36}$$

where Y_i corresponds to L^*_i, $i = 1,\ldots,n$.

All anchor points are located on the line section between $v_{r,\min}$ and $v_{r,\max}$ and therefore in the convex set M^c_{XYZ}.

Direction Vector v

The direction vectors have to be calculated for each MBD matrix entry. Due to the structure of the MBD their Y components equal zero.

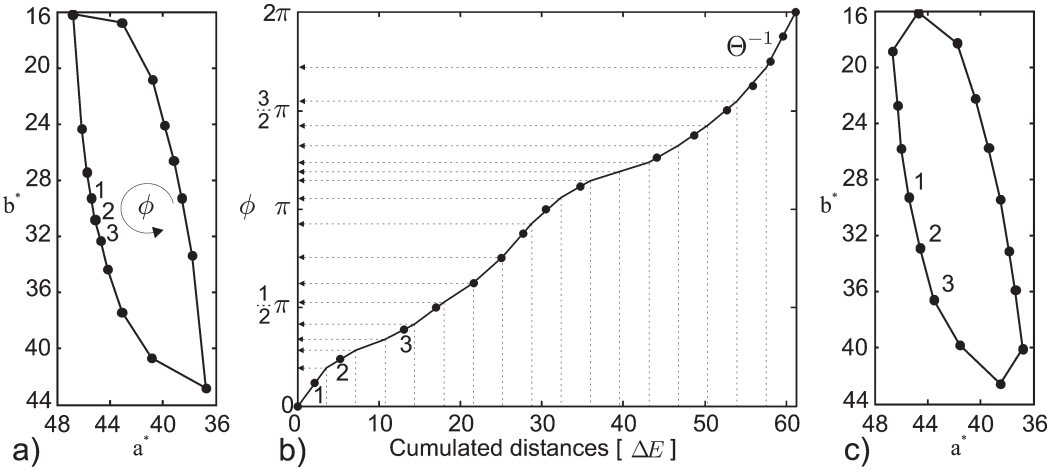

Figure 3. a) Contour plot of the metamer subspace at a fixed luminance level. Equidistant angles result in a non-uniform distribution of the points on the contour. b) The inverse of Θ shows the angles which result in a nearly uniform distribution of the contour points. These points are shown in c).

For each luminance level, which is defined by an anchor point, we choose the direction vectors in such a way, that they uniformly cover the contour of M^c_{XYZ}. We therefore use a multigrid strategy. Initially we take a decomposition of $[0, 2\pi]$

$$\phi_k := \frac{2\pi k}{K}, \quad k = 0,...,K, \tag{37}$$

and the appropriate direction vectors

$$v_k := \begin{bmatrix} \cos(\phi_k) \\ 0 \\ \sin(\phi_k) \end{bmatrix}, \quad k = 0,...,K \tag{38}$$

in order to calculate $K + 1$ boundary points of M^c_{Lab}, using the LP problem, Eqs. (16) through (24). In general the resulting boundary points $\mathcal{L}(v_{r,k})$, $k = 0,...,K$ are not distributed uniformly on the contour of M^c_{Lab} at the fixed luminance level (see Fig. 3(a)).

If we assign a cumulative distance to each angle ϕ_k, $k = 0,...,K$

$$\phi_0 \to \xi_0 := 0 \tag{39}$$

$$\phi_k \to \xi_k := \sum_{j=1}^{k} \Delta E(\mathcal{L}(v_{r,j-1}), \mathcal{L}(v_{r,j})) \tag{40}$$

we can define a function $\Theta : [0; 2\pi] \mapsto \mathbb{R}^+$ by linear interpolation of the resulting pairs. This function is strictly monotonicly increasing and therefore invertible. We can then define new angles by inverting Θ (see Fig. 3(b))

$$\tilde{\phi}_i := \Theta^{-1}\left(\frac{i}{m}\xi_K\right), \quad i = 1,...,m. \tag{41}$$

The corresponding direction vectors, which are defined by Eq. (38), result in boundary points which are more uniformly distributed on the contour of M^c_{Lab} at the appropriate luminance level. If we repeat this procedure, we obtain points which are distributed more uniformly. In our simulation experiments we used only one iteration step.

Noise Considerations

If we consider noisy systems, the LP problems embodied in contraints (16) through (24) and (26) through (33), may not be solvable because the set defined by the constraints is empty. In the case of such systems we can ensure solvability by introducing the unknown noise $\varepsilon \in \mathbb{R}^n$ $(\varepsilon \neq 0)$ in constraints (21) and (32)

$$\Omega_a r = c + \varepsilon \tag{42}$$

as an additional arbitrary variable. The size of this variable is bounded by other arbitrary variables $\Delta\varepsilon = (\Delta\varepsilon_1,...,\Delta\varepsilon_n)^T \in \mathbb{R}^n$ in further constraints

$$\Delta\varepsilon \geq \varepsilon \tag{43}$$

$$\Delta\varepsilon \geq -\varepsilon \tag{44}$$

$$\Delta\varepsilon \geq 0 \tag{45}$$

$$\Delta\varepsilon \leq \xi. \tag{46}$$

Constraints (43) and (44) restrict the magnitude of the noise and can be combined into $|\varepsilon| \leq \Delta\varepsilon$. The next two constraints (45) and (46) force the noise inside the noise outlier set,[12,20] where $\xi = 3\sigma_\varepsilon$ is used for Gaussian noise (σ_ε describes the standard deviation of the noise and 99.7% of the values are at most three standard deviations away from the mean if we consider Gaussian noise). It is also possible to use more complex noise models, including shot noise, which follows Poisson statistics. If there is a large number of detected photons, then the signal can be well modeled by a signal-dependent gaussian distribution, where the variance is equal to the mean.[29] This noise model can be expressed as follows.[30]

$$c^{\text{noise}} = \Omega_a r + f(c^{\text{noise}}) \circ \varepsilon_S + \varepsilon_t \tag{47}$$

$$= \Omega_a r + (f(c_1^{\text{noise}}) \cdot \varepsilon_{s1}, \ldots, f(c_n^{\text{noise}}) \cdot \varepsilon_{sn})^T + \varepsilon_t, \tag{48}$$

where ε_t represents the zero mean gaussian distribution of the thermal noise and $f(c^{\text{noise}}) \circ \varepsilon_s$ represents the shot noise. Signal dependency is modeled by $f(c^{\text{noise}})$ and ε_s has a zero mean gaussian distribution. ε_t and ε_s can be treated as independent. Constraint (46) can be modified to consider this signal-dependent noise model by setting $\xi(c^{\text{noise}}) = 3\sigma_{\varepsilon_{st}}(c^{\text{noise}})$, where

$$\sigma_{\varepsilon_{st}}(c^{\text{noise}}) = \sqrt{f(c^{\text{noise}})^2 \sigma_{\varepsilon_s}^2 + \sigma_{\varepsilon_t}^2}$$

is the standard deviation of the signal-dependent gaussian distribution of the noise model.

As the thresholds $\Delta\varepsilon \in \mathbb{R}^n$ are unknown *a priori*, they are minimized in the objective function using an additional weighted term. The objective function (16) will be replaced by

$$-\lambda + w_\varepsilon \cdot \sum_{i=1}^{n} \Delta\varepsilon_i = \min \tag{49}$$

and the objective functions (26) and (27) are changed to

$$-v_r^Y r + w_\varepsilon \cdot \sum_{i=1}^{n} \Delta\varepsilon_i = \min \tag{50}$$

$$v_r^Y r + w_\varepsilon \cdot \sum_{i=1}^{n} \Delta\varepsilon_i = \min, \text{ resp.} \tag{51}$$

The weight $w_\varepsilon > 0$ should be large enough to ensure that the solution contains $\varepsilon \approx 0$ in the case of a noise-free system. In our simulation experiments with noise free systems $w_\varepsilon = 1000$ leads to the same results as a calculation without any consideration of noise.

Approximating the Optimal Color Correction Transformation

When a Metamer Boundary Descriptor for a sensor response c has been determined, the optimal color correction transformation with respect to the ΔE^*_{ab} can be approximated by calculating the center of gravity of the MBD matrix entries. Equal matrix entries are considered only once. If $d_1, \ldots, d_k \in M^c_{Lab}$, $k \leq m \cdot n$ are the pairwise different matrix entries an approximating solution can be calculated as follows

$$C(c) \approx \frac{1}{k} \sum_{i=1}^{k} d_i. \tag{52}$$

This first approximation can be improved by a better consideration of the shape of M^c_{Lab}. Equation (52) weights all boundary points equally which are stored in the MBD matrix regardless of their position. The aim is not to calculate the center of gravity of the MBD matrix entries but the center of gravity of the metamer subspace M^c_{Lab} itself, i.e.,

$$C(c) \approx \frac{1}{\text{Vol}(M^c_{Lab})} \int_{M^c_{Lab}} \begin{bmatrix} L^* \\ a^* \\ b^* \end{bmatrix} dL^* a^* b^*. \tag{53}$$

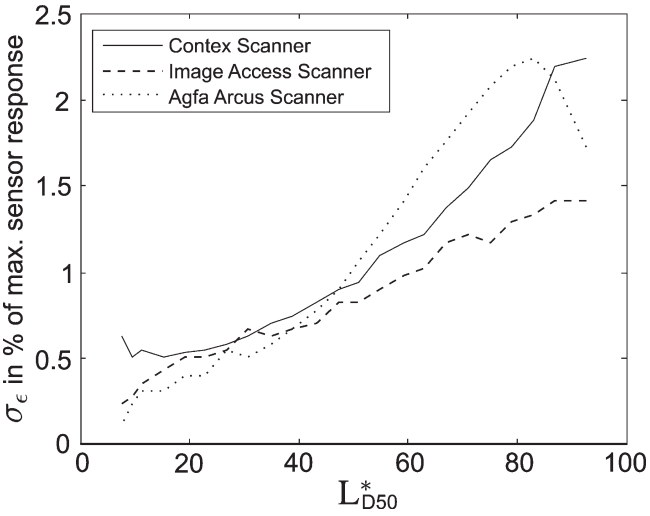

Figure 4. Signal dependency of noise (green channel) of three different scanners calculated for the gray ramp of an IT8.7/2 Target.

Vol(M^c_{Lab}) denotes the volume of M^c_{Lab}. In Appendix B, available as Supplemental Material, we describe how to calculate the integral in Eq. (53). Hence the center of gravity is not always part of the considered set it should be mentioned that in our experiments the calculated point always lies inside M^c_{Lab}.

Results

We have compared our method (MBD) with the methods described in the introduction by means of simulation. These methods were selected for various reasons. The MPR target based methods are often used and compared with one another,[3,5,31] The RM method allows for noise. As we also take noise into account in acquisition systems, a comparison with this method could be interesting. The LPCC method[15] is based on the same assumptions as the MBD method, while the POCS method belongs to the model-based methods and also allows for noise.

We carried out four different simulation experiments to compare the methods using different simulation parameters: In Simulation I we used a Sony RGB sensor[32] with sensitivities shown in Fig. 5. In Simulation II we used the same sensor but added ±1% of the maximum sensor response as noise to each channel. This signal independent noise is not typical of a special image aqcuisition system. As mentioned above acquisition systems normally have a more complex signal dependent noise behavior.[29,30] Measurements of IT 8.7/2 targets by different scanners (see Fig. 4) have shown that the standard deviation of noise has a mean magnitude of approximately 1% of the maximum sensor response. Our aim was to review each method with respect to disturbed sensor responses, i.e., how the methods amplify or mute noise. The disturbing magnitude of ±1% of the maximum sensor response per channel was also selected by König[5] in his simulation experiments.

In Simulation III we used an experimental six channel sensor[5,31] with sensitivities shown in Fig. 6. In Simulation IV we used the same sensor but added ±1% of the maximum sensor response as noise to each channel.

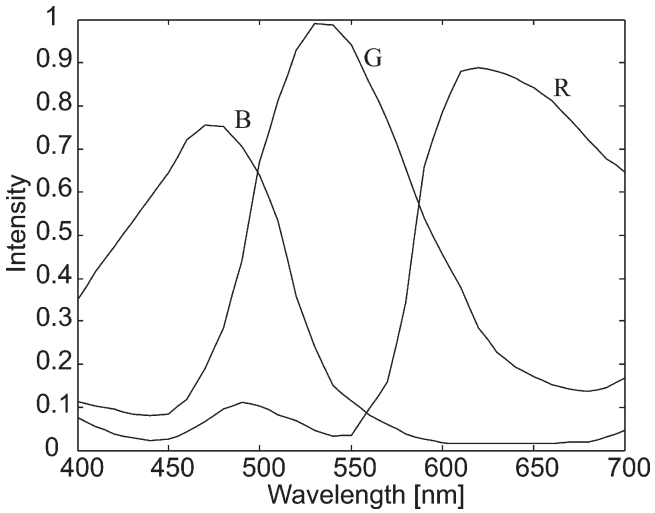

Figure 5. Sensitivities of the Sony RGB Sensor[32]

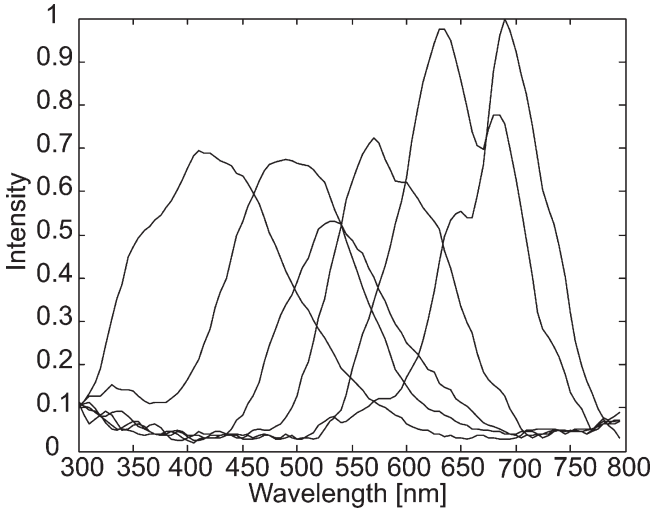

Figure 6. Sensitivities of the experimental six channel sensor.[5,31]

TABLE I. Simulation Parameters

	Simulation I	Simulation II	Simulation III	Simulation VI
Sensor	Sony RGB	Sony RGB	6 Channel	6 Channel
Acquisition Illuminants	A,C,F11	A,C,F11	A,C,F11	A,C,F11
Viewing Illuminants	A,C,F11	A,C,F11	A,C,F11	A,C,F11
Noise	–	1% of the max. sensor response per channel	–	1% of the max. sensor response per channel
Test Spectra	Vrhel,IT 8.7/2	Vrhel,IT 8.7/2	Vrhel,IT 8.7/2	Vrhel,IT 8.7/2
Spectral sampling	5 nm	5 nm	5 nm	5 nm

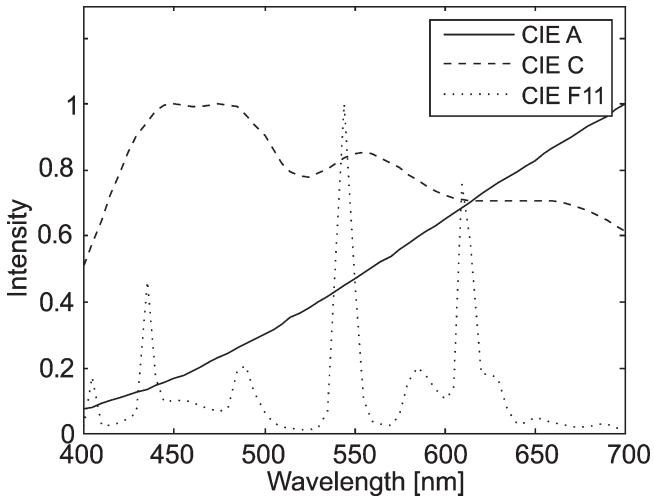

Figure 7. Acquisition and viewing illuminants used in simulation experiments.

The acquisition and viewing illuminants have been chosen as CIE-A (incandescent light, color temperature: 2856°K), CIE-C (average daylight, color temperature: 6774°K), CIE-F11 (narrow band white fluorescent lamp) (see Fig. 7). For each simulation we calculated the color corrections for all combinations of acquisition and viewing illuminants.

The test colors used in each simulation consisted of two different spectral databases, i.e., a spectrally measured IT8.7/2 target[33] with 288 color patches and the Vrhel database,[34] including 354 reflection spectra broken down into three groups (*Dupont*: 120 Dupont paint chips, *Munsell*: 64 Munsell chips and *Objects*: 170 natural and man-made objects). The IT8.7/2 test spectra differ from the IT8.7/2 spectra used as training colors for the target based methods. However, both IT8.7/2 spectral sets are highly correlated (correlation coefficient 0.97).

A test database which is highly correlated with the training colors and a different spectrally higher dimensional[35] test database were chosen in order to test the generalization ability of the target based methods.

Determination of the coefficients of the multi-order polynomials or the RM entries using measured target patches is disturbed by noise in actual practice. For the same reason the acquisition lighting matrix cannot be calculated in an error free way for real acquisition systems, e.g., by measurement or by using the methods listed above. The authors are aware of the fact that the results of this simulation could be different if the parameters of the methods used were estimated on the basis of noisy data. An estimation of these parameters is not within the scope of the text. The parameters we selected for the color correction methods were therefore error free in this simulation.

The simulation parameters are summarized in Table I and the parameters needed for the methods are shown in Table II. The LPCC method is based on the assumption that all natural reflection spectra can be modeled by a few basis spectra which can be extracted from a representative spectral database. These basis spectra have been calculated for our simulations using 99% of the energy of 1269 munsell color chips* which result in 25 basis spectra. As already mentioned we chose an IT8.7/2 target[33] for the training colors of the target based methods. This target is widely used to create ICC profiles[36] for scanners or cameras in practice.

* The Munsell spectra are available from the Information Technology Dept., Lappeenranta University of Technology, Finland.

TABLE II. Parameters of Methods in Simulation I-IV. Symbols Correspond to Previous Definitions

	Target	Parameter
MBD	–	MBD matrix rows: n = Round [2 ($L^*_{max} - L^*_{min}$) + 0.5] MBD matrix columns: $m = 8$ Smoothness parameter: $\rho = 0.0035$ Max. noise amplitude: $\xi = 0.03$
MPRXYZ	IT 8.7/2	Polynomial order: $p = 3$
MPRLabH	IT 8.7/2	Polynomial order: $p = 3$
MPRLabK	IT 8.7/2	Polynomial order: $p = 3$
RM	IT 8.7/2	–
LPCC	–	Basis of reflection spectra consists of 25 spectra which include 99.0% of the energy of 1269 reflection spectra of Munsell color chips.
POCS	–	Convex sets: 1. $r \geq 0$ (positivity) 2. $r \leq 1$ (boundness) 3. $\|Hr\| \leq 0.0035$ (smoothness) 4. $\|\Omega_s r - (c + \varepsilon)\| \leq 0$ (Simulation I + III) or $\|\Omega_s r - (c + \varepsilon)\| \leq 0.01$ (Simulation II + IV) Exit condition: $\|r^i - r^{i+1}\|_2 \leq 10^{-5}$ or $i > 100000$

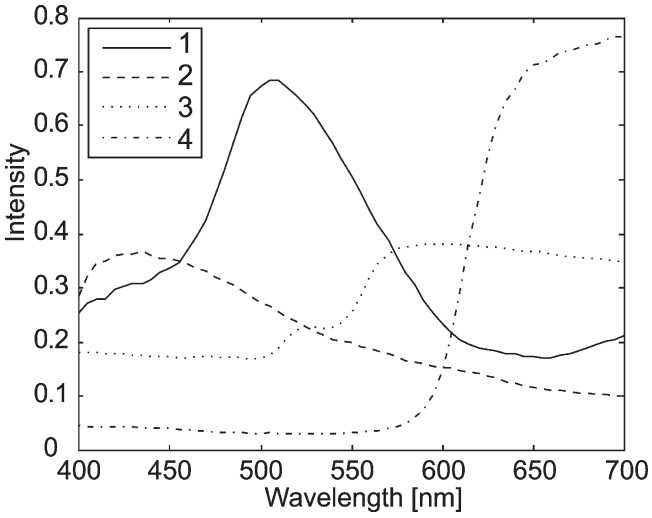

Figure 8. Examples of some Munsell spectra extracted from the Vrhel database

The results achieved for Simulations I-IV are shown in Tables III through VI. Figures 12 through 15 show the results for the Vrhel database which are broken down according to the analyzed illuminants.

A few examples of the metamer subspace structures can be found in Figs. 9 and 10 for the spectra shown in Fig. 8.

Discussion

The results for Simulation I using the IT8.7/2 test spectra demonstrate that the MPR methods perform very well for test colors which are highly correlated with the training colors. There is no advantage in using the nearly perceptual uniform CIE L*a*b* space for regression. The MBD method follows with a mean ΔE_{ab} difference of nearly 1 compared with the best MPR method (MPRXYZ). For the Vrhel test spectra the MBD method surpasses all other methods. The MPR methods are clearly worse than in the case of the IT8.7/2 colors and follow with a difference of nearly $\Delta E^*_{ab} = 0.7$ after the MBD method. The different spectral test databases have no visible influence on the model based methods (MBD, LPCC, POCS). The LPCC performs a little worse than the MPR methods and the POCS method results in very large mean errors bigger than $\Delta E^*_{ab} = 10$. This is due to the large magnitudes of the metamer subspaces for the three channel Sony sensor. The RM method also shows high error rates which are obviously smaller for the IT8.7/2 test colors. This difference in error rate is also due to the different correlation between test colors and training colors.

In Simulation II the MBD method results in the smallest mean ΔE^*_{ab} errors for both spectral test databases considered. For the IT8.7/2 test colors the MBD method is followed by the MPR methods, while for the Vrhel colors the LPCC method is the second best procedure after the MBD method. As seen in Simulation I the target based methods show the same different error behavior in both of the spectral test databases. In this case as well the MPR methods do not show any noticeable differences. The conspicuous noise sensitivity of the MPR methods seen in Simulation IV is less obvious for the Sony RGB sensor. Nevertheless, this

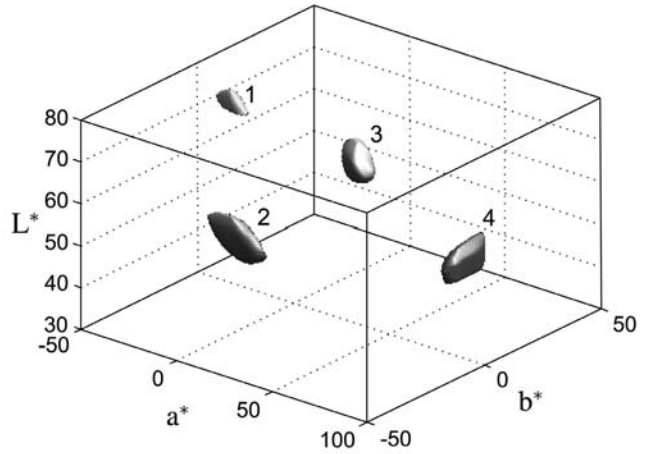

Figure 9. Metamer subspaces of the spectra in Fig. 8 under viewing illuminant C calculated for the Sony sensor with acquisition illuminant F11.

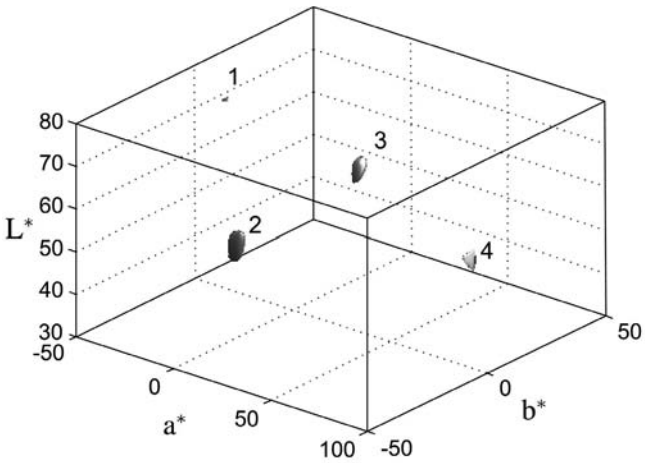

Figure 10. Metamer subspaces of the spectra in Fig. 8 under viewing illuminant C calculated for the experimental six channel sensor with acquisition illuminant F11.

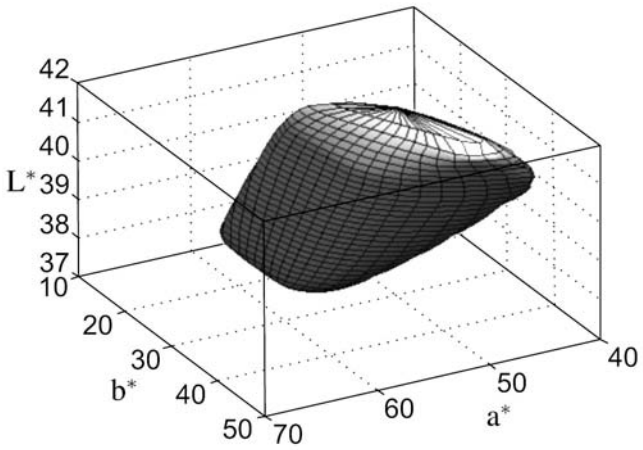

Figure 11. Detailed view on metamer subspace no. 4 in Fig. 9 (different perspective)

TABLE III. Results for Simulation I (Sony RGB, No Noise). Values Refer to All Illuminants

	IT 8.7/2			Vrhel		
	$E(\Delta E^*_{ab})$	$\text{Std}(\Delta E^*_{ab})$	$\text{Max}(\Delta E^*_{ab})$	$E(\Delta E^*_{ab})$	$\text{Std}(\Delta E^*_{ab})$	$\text{Max}(\Delta E^*_{ab})$
MBD	4.58	2.83	23.20	5.05	3.59	36.98
MPRXYZ	3.72	1.56	21.08	6.62	5.31	54.10
MPRLabH	3.84	1.62	16.35	6.02	4.14	44.88
MPRLabK	3.93	1.74	21.52	5.70	3.95	40.88
RM	9.46	7.45	48.58	14.16	10.86	74.34
LPCC	6.21	3.56	28.93	6.55	5.70	59.99
POCS	12.44	6.63	51.46	13.68	6.73	67.66

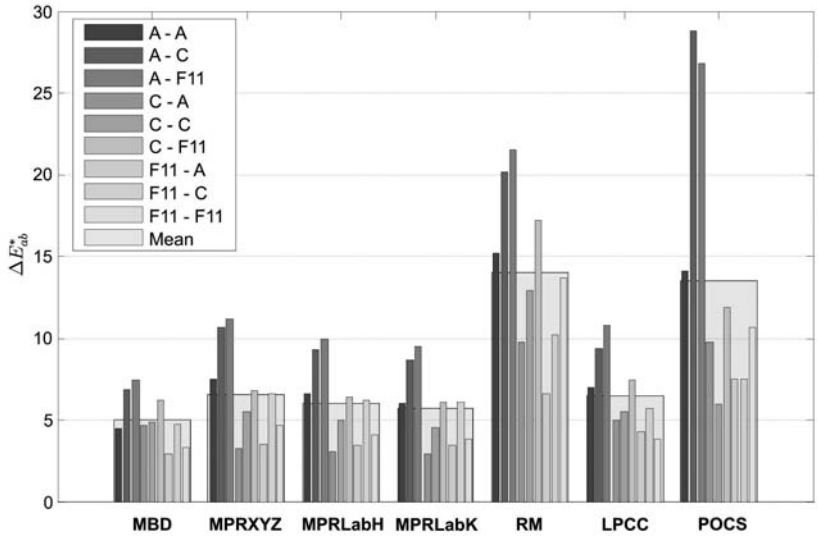

Figure 12. Results for the Sony RGB sensor (noise free). Values refer to the Vrhel database.

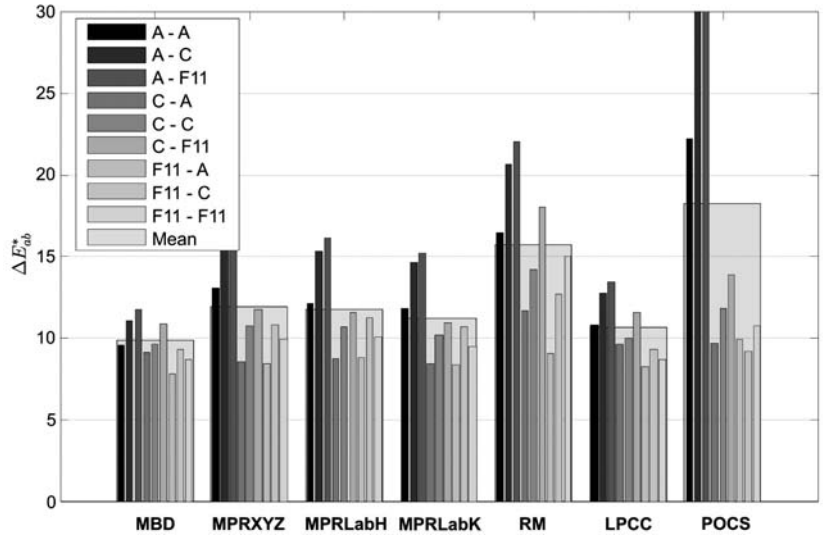

Figure 13. Results for the Sony RGB sensor (1% noise). Values refer to the Vrhel database.

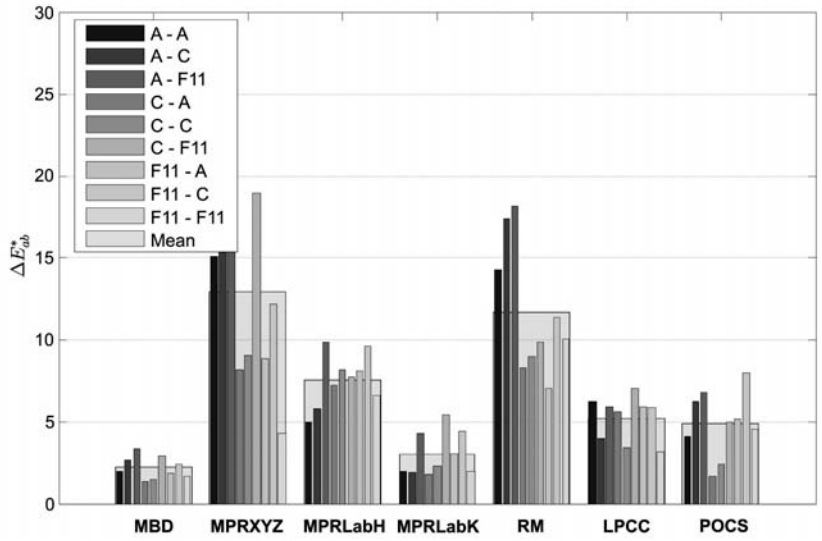

Figure 14. Results for the six channel sensor (0% noise). Values refer to the Vrhel database.

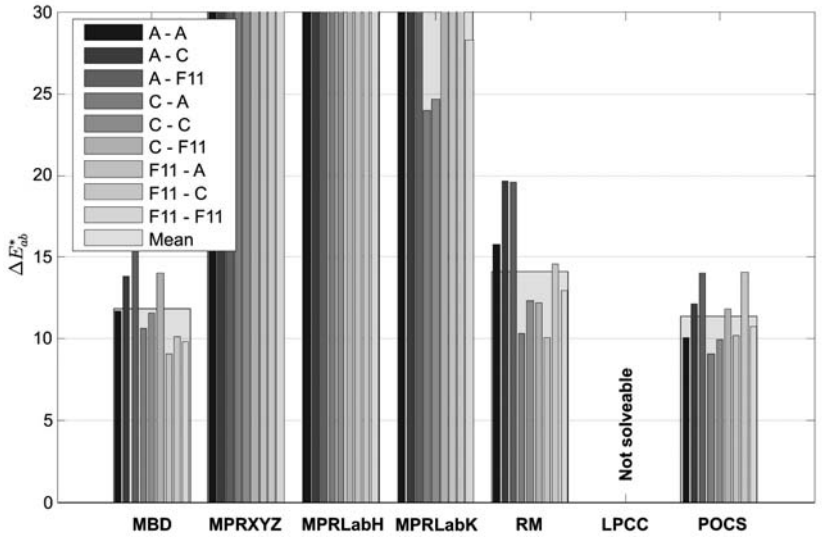

Figure 15. Results for the six channel sensor (1% noise). Values refer to the Vrhel database.

TABLE IV. Results for Simulation II (Sony RGB, 1% Noise). Values Refer to All Illuminants

	IT 8.7/2			Vrhel		
	$E(\Delta E^*_{ab})$	Std(ΔE^*_{ab})	Max(ΔE^*_{ab})	$E(\Delta E^*_{ab})$	Std(ΔE^*_{ab})	Max(ΔE^*_{ab})
MBD	8.13	5.21	27.47	9.77	7.98	97.42
MPRXYZ	8.50	6.28	50.90	11.83	9.95	80.84
MPRLabH	8.52	6.17	42.64	11.65	10.41	157.21
MPRLabK	8.54	6.17	42.70	11.10	9.24	93.92
RM	10.73	7.49	50.37	15.57	11.11	75.66
LPCC	9.46	5.41	34.33	10.50	7.88	63.12
POCS	15.97	9.11	86.46	18.08	10.00	109.84

TABLE V. Results for Simulation III (6 Channel, No Noise). Values Refer to All Illuminants

	IT 8.7/2			Vrhel		
	$E(\Delta E^*_{ab})$	Std(ΔE^*_{ab})	Max(ΔE^*_{ab})	$E(\Delta E^*_{ab})$	Std(ΔE^*_{ab})	Max(ΔE^*_{ab})
MBD	1.83	3.26	13.21	2.21	2.05	21.53
MPRXYZ	3.55	9.60	32.28	12.95	18.03	278.93
MPRLabH	4.48	2.44	21.35	7.60	7.18	104.11
MPRLabK	0.86	0.60	7.00	3.03	2.99	76.53
RM	7.26	6.13	47.63	11.73	9.99	73.20
LPCC	2.58	2.20	23.38	5.26	7.51	77.20
POCS	3.61	1.76	14.71	4.90	2.85	29.66

TABLE VI. Results for Simulation IV (6 Channel, 1% Noise). Values Refer to All Illuminants

	IT 8.7/2			Vrhel		
	$E(\Delta E^*_{ab})$	$\mathrm{Std}(\Delta E^*_{ab})$	$\mathrm{Max}(\Delta E^*_{ab})$	$E(\Delta E^*_{ab})$	$\mathrm{Std}(\Delta E^*_{ab})$	$\mathrm{Max}(\Delta E^*_{ab})$
MBD	11.46	9.53	70.92	11.88	9.76	77.76
MPRXYZ	> 50	> 50	> 100	> 50	> 50	> 100
MPRLabH	> 50	> 50	> 100	> 50	> 50	> 100
MPRLabK	29.85	23.07	> 100	34.07	26.81	> 100
RM	9.34	6.19	46.16	14.18	10.25	72.70
LPCC	–	–	–	–	–	–
POCS	11.40	8.62	54.12	11.35	8.93	71.44

seems to be the reason why the MPR methods result in bigger errors for the IT8.7/2 colors than the MBD method. Unlike Simulation I they are surpassed by the LPCC method for the Vrhel colors. The RM method leads to almost the same results as in Simulation I. The results show the second worst error rates and are only exceeded by the POCS method. Allowing for noise in the RM and POCS methods does not seem to have any benefit for the Sony RGB sensor compared with the other methods.

In Simulation III the error rates of all the methods are lower than in Simulation I. This is due to the smaller metamer subspaces of the six channel sensor compared to the Sony RGB sensor (see Figs. 9 and 10). This simulation shows a distinct difference between the MPR methods which is very noticeable in the case of the Vrhel colors. The regression in the CIE L*a*b* color space has obvious benefits, as shown by the excellent mean error of the MPRLabK method of $\Delta E^*_{ab} = 0.86$ using the IT8.7/2 colors. The MBD method show the second best results for the IT8.7/2 colors and again the best results in the case of the Vrhel colors. Due to the smaller metamer subspaces the LPCC and the POCS methods have relatively small error rates and are better than the MPRXYZ and MPRLabH methods. This simulation also demonstrates a major difference between the error rates of the target based methods with respect to the test color databases used. Once again this is the result of the correlation with the training colors.

Simulation IV shows that the MPR methods considerably amplify the influence of noise due to their higher order terms in the polynomials. MPR methods are therefore not usable for noisy systems with many channels. The absense of any allowance for noise in the LP problems of the LPCC method leads to an empty constraint set in the case of various sensor responses, i.e., the method cannot be used. This behavior was not observed in Simulation II for the Sony RGB Sensor.

The strength of the RM method is evident in the presence of noise in the 6 channel system. For the IT8.7/2 colors the smallest mean errors are obtained with the RM method. The MBD and POCS methods outperform the other methods with respect to the Vrhel colors and result in similar error rates. This demonstrates that selecting the center of gravity of small metamer subspaces in noisy systems offers no evident benefits compared with the choice of an arbitrary color as in the POCS method.

Finally these simulation experiments demonstrates that the **MBD** method is one of the most precise methods for all of the analyzed noise-free systems as well as for all noisy systems. All of the other investigated methods have their strengths only in one of these cases.

A drawback of the MBD method compared with the other methods is its numerical complexity. To calculate the MBD matrix 2 nm + 2 linear programming problems have to be solved, using one iteration step to determine the half line parameters. The MBD matrix in our simulation experiments using an Athlon64 CPU, Matlab[27] and non time optimized code is calculated on the average in 10 seconds. The computation of many color corrections, e.g., for all pixels of a high-resolution image, is therefore very time consuming on standard hardware.

Conclusion

A new model based method for color correction was presented and compared with other methods by simulation experiments. The new method characterizes the metamer subspace of reflection spectra, which result in the given sensor response, by calculating a metamer boundary descriptor matrix in the CIE L*a*b* color space. Using a larger matrix dimension we obtain a better representation of the metamer subspace. By calculating the center of gravity of all different matrix entries we achieve a good approximation of the color with the smallest mean ΔE distance to all other possible colors so that this is a good choice for achieving small mean errors in color correction. The results also validate the performance of our method for noisy systems.

References

1. G. Sharma, *Digital Color Imaging Handbook*, (CRC PRESS, Boca Raton, FL, 2003), p. 82.
2. F. König and P. G. Herzog, "On the limitations of metameric imaging", *Proc. IS&T's PICS: Image Processing, Image Quality, Image Capture, Systems Conference*, (IS&T, Springfield, VA, 1999), p. 163.
3. J. Y. Hardeberg, *Acquisition and Reproduction of Colour Images: Colorimetric and Multispectral Approaches*, PhD thesis, (Ecole Nationale Supérieure des Télécommunications, France, 1999).
4. R. Berns, *Billmeyer and Saltzman's: Principles of Color Technology*, 3rd ed., (John Wiley and Sons, Inc., New York, 2000).
5. F. König, *Die Charakterisierung von Farbsensoren*, PhD thesis, (Rheinisch-Westfälische Technische Hochschule Aachen, Deutschland, 2001).
6. M. J. Vrhel and H. J. Trussell, "Color scanner calibration via a neural network", *Proc. IEEE ICASSP-99*, ISSN: 0-7803-5041-3, **6,** 3465–3468 (1999).
7. P.-C. Hung, "Colorimetric calibration for scanners and media", *Proc. SPIE* **1448,** 164–174 (1991).
8. G. D. Finlayson and M. S. Drew, "Constrained least-squares regression in color spaces", *J. Electronic Imaging* ISSN: 1017-9909, **6,** 484 (1997).
9. F. H. Imai, R. S. Berns and D.-Y. Tzeng, "A Comparative Analysis of Spectral Reflectance Estimated in Various Spaces Using a Trichromatic Camera System", *J. Imaging Sci. Technol.* ISSN: 1062-3701, **44,** 280 (2000).
10. G. Wyszecki and W. Stiles, *Color Science: Concepts and Methods, Quantitative Data and Formulae*, 2nd ed.,(John Wiley and Sons, Inc., New York, 2000), p. 183ff.
11. H. J. Trussell, "Applications of set-theoretic methods to color systems", *Color Res. Appl.* ISSN: 0361-2317, **16,** 31 (1991).
12. G. Sharma and H. J. Trussell, "Set theoretic estimation in color scanner characterization", *J. Electronic Imaging* ISSN: 1017-9909, **5,** 479 (1996).
13. G. Sharma, "Targetless scanner color calibration", *J. Imaging Sci. Technol.* ISSN: 1062-3701, **44,** 301 (2000).
14. G. Sharma, "Set theoretic estimation for problems in subtractive color", *Color Res. Appl.* ISSN: 0361-2317, **25,** 333 (2000).
15. G. D. Finlayson and P. M. Morovic, "Metamer constrained color correction", *J. Imaging Sci. Technol.* ISSN: 1062-3701, **44,** 295 (2000).
16. M. S. Drew and B. V. Funt, "Natural metamers", in *CVGIP: Image understanding*, ISSN 1049-9660, **56**, 139–151 (1992) .
17. G. D. Finlayson and P. Morovic, "Error less colour correction", in *ICPR 2004*, (IEEE, Cambridge, UK, 2004), pp. 181–185.
18. G. D. Finlayson and P. Morovic, "Intensity constrained error-less colour correction", *Proc. IS&T/SID Color Imaging Conf.*, (IS&T, Springfield, VA, 2004) pp. 106–110.
19. W. K. Pratt, *Digital Image Processing*, vol. 2, (John Wiley and Sons, Inc., New York, 1991), p. 383 ff.
20. G. Sharma and H. J. Trussell, Characterization of scanner sensitivity, *Proc. IS&T/SID Color Imaging Conf.*, (IS&T, Springfield, VA, 1993) pp. 103–107.

21. G. D. Finlayson, S. Hordley and P. M. Hubel, "Recovering device sensitivities with quadratic programming", *Proc. IS&T/SID Color Imaging Conf.*, (IS&T, Springfield, VA, 1998), pp. 90–95.
22. J. B. Cohen and W. E. Kappauf, "Metameric color stimuli, fundamental metamers, and Wyszecki's metameric blacks", *Amer. J. Psychology* ISSN: 0002-9556, **95,** 537 (1982).
23. J. B. Cohen and W. E. Kappauf, "Color mixture and fundamental metamers: Theory, algebra, geometry, application", *Amer. J. Psychology* ISSN: 0002-9556, **98,** 171 (1985).
24. W. Stiles, G. Wyszecki and N. Ohta, "Counting Metameric Object-color stimuli using frequency-limited spectral reflectance functions", *J. Opt. Soc. Amer.* ISSN: 0030-3941, **67,** 779 (1977).
25. W. Praefcke, "Transform Coding of Reflectance Spectra Using Smooth Basis Vectors:, *J. Imaging Sci. Technol.* ISSN: 1062-3701, **40,** 543 (1996).
26. N. Ohta and G. Wyszecki, "Theoretical chromaticity mismatch limits of metamers viewed under different illuminants", *J. Opt. Soc. Amer.* ISSN: 0030-3941, **65,** 327 (1975).
27. MATLAB, *The Language of Technical Computing, Language Reference Manual*, 6th ed., (The MathWorks Inc., Natick, MA, 2001).
28. S. Mehrotra, "On the Implementation of a Primal-Dual Interior Point Method", *SIAM J. Optimization* ISSN: 1052-6234, **2,** 575 (1992).
29. W. K. Pratt, *Digital Image Processing*, vol. 1, (John Wiley and Sons, Inc., New York, 1978) p. 367.
30. M. Vrhel and H. J. Trussell, "Optimal color filters in the presence of noise", *IEEE Trans. Image Processing* ISSN: 1057-7149, **4,** 814 (1995).
31. P. G. Herzog, D. Knipp, H. Stiebig, and F. König, "Colorimetric characterization of novel multiple channel sensors for imaging and metrology", *J. Electronic Imaging* ISSN: 1017-9909, **8,** 342 (1999).
32. Sony, ICX434DQN, Diagonal 5.68mm (Type 1/3.2) Frame Readout CCD Image Sensor with Square Pixel for Color Cameras, Datasheet.
33. NPES, Graphic technology - color reflection target for input scanner calibration, volume IT8.7/2-1993, Reston, Virginia, 1999.
34. M. Vrhel, R. Gershon and L. Iwan, "Measurement and analysis of object reflectance spectra", *Color Res. Appl.* ISSN: 0361-2317, **19,** 4 (1994).
35. J. Y. Hardeberg, "On the spectral dimensionality of object colours", *Proc. CGIV*, (IS&T, Springfield, VA, 2002) pp. 480–485.
36. ICC, File Format for Color Profiles, http://www.color.org, 4.0.0 edition, 2002.
37. B. Korte and J. Vygen, *Combinatorial Optimization*, 1st ed., (Springer-Verlag, Berlin, Germany, 1991).
38. P. Urban and R.-R. Grigat, "Color correction by calculating a metamer boundary descriptor", *Proc CGIV*, (IS&T, Springfield, VA, 2004) pp. 536–541.